Implementation of the interacting quantum atoms energy decomposition with the CASPT2 method

Jesús Jara Cortés,*,† Edith Leal-Sánchez,‡ Evelio Francisco,¶ José A. Pérez-Pimienta,† Ángel Martín Pendás,¶ and Jesús Hernández-Trujillo‡

†*Unidad Académica de Ciencias Básicas e Ingenierías, Universidad Autónoma de Nayarit, Tepic, 63155, México.*

‡*Departamento de Física y Química Teórica, Facultad de Química, UNAM, México City 04510, México*

¶*Departamento de Química Física y Analítica, Faculta de Química, Universidad de Oviedo, Oviedo 33006, Spain.*

E-mail: josejc@uan.edu.mx

Phone: (52) 311-211-8800

Abstract

We present an implementation of the interacting quantum atoms energy decomposition scheme (IQA) with the complete active space second-order perturbation theory (CASPT2). This combination yields a real-space interpretation tool with the proper account of static and dynamic correlation that is particularly relevant for the description of processes in electronic excited states. The IQA/CASPT2 approach allows to determine the energy redistribution that takes place along a photophysical/photochemical deactivation path in terms of self- and interatomic contributions. The applicability of the method is illustrated by the description of representative processes spanning different bonding regimes: noble gas excimer and exciplex formation, the reaction of ozone with a chlorine atom, and the photodissociations of formaldehyde and cyclobutane. These examples show the versatility of using CASPT2 with the significant information provided by the IQA partition to describe chemical processes with large multiconfigurational character.

Introduction

The enormous power of modern computational chemistry should, by no means, obscure the fact that most advances in Chemistry rely on the manipulation of a set of core chemical bonding concepts so deeply rooted in the chemist's mind that they pass normally unnoticed. Most of these concepts were organized around the vast experience accumulated over the years in ground states, and cannot be easily generalized, or simply do not work at all when we leave this realm. Building chemical intuition in excited states requires methods to analyze, with a chemical eye, the results of high-level calculations, since low quality methodologies normally do not provide sufficient accuracy. When one leaves the single-determinant ansatz this is not an easy enterprise. In this sense, chemically insightful energy decomposition schemes play an important role, because they can be used directly to explain the observed changes in the potential energy surfaces (PES) of reaction processes.[1] Among the most important

schemes currently in use, the interacting quantum atoms method (IQA)[2] provides a detailed description about the interactions among the atoms in a molecule and has been used to study of a diversity of chemical processes in ground state.[3–6]

On top of a proper PES information obtained from an electronic structure method, the IQA approach provides a theoretical framework for the study of systems in excited electronic states, which can be useful for the mechanistic rationalization of photochemical or photophysical processes. To mention a few instances, it allows to analyze how the energy is redistributed locally after an electronic transition, as well as to describe which are the energetic contributions that drive the relaxation of an excited molecule.[7] It also allows to characterize the nature of interactions in the formation of excimers and exciplexes. Moreover, it allows to identify which are the contributions of the atomic and interaction terms to the energy barriers along a minimum energy path, for example when accessing from an equilibrium geometry to a minimum energy conical intersection.

One of the main advantages of IQA, in contrast to the virial based atomic energies, is that the partition can be carried out at any point on the potential energy surface, involving structures other than equilibrium geometries. Additionally, the analysis is applicable to intra- and intermolecular cases, so can be performed hierarchically from atoms, molecules or aggregates. In addition, it does not require the introduction of arbitrary reference states to perform the analysis. In contrast to other energy partitioning schemes such as SAPT or EDA,[8,9] these features make the use of IQA appealing for the study of excited state processes. For example, there is no currently a computational SAPT implementation to deal with excited states, and there are problems in defining fragments and reference states within EDA to calculate excited states of systems other than intermolecular complexes.

Despite the above, the number of studies reporting the use of the IQA partition in the excited state is scarce. Among them, Fernandez-Alarcón et al. performed the analysis of the vertical transition energies of a group of small molecules, thus making it possible to dissect the excitation energies and quantify the contribution of each atom and functional

group to the observed value.[7] As another example, IQA has been used to rationalize how the hydrogen bonding in $(H_2O)_2$ gives rise to the hypso- and bathochromic shifts with respect to the excitation energy of the isolated monomers.[10] Moreover, Jara-Cortés et al. performed a study for some representative excited systems, to describe the bond breaking, excimers, charge transfer complexes, as well as the energetic redistribution in the neighbourhood of a conical intersection in a perspective centered on the charge density.[11] In general, it has been shown how these techniques allow to complement with quantitative data the information provided by the analysis of molecular orbitals.[12]

Although the IQA machinery is conceptually simple, in order to carry out the energetic decomposition with a particular electronic structure method it is necessary to obtain the first and second order density matrices, properties that are only well defined for configuration interaction approaches. In the case of Coupled Cluster and Moller-Plesset methods (CCSD and MP2), the density matrices can be evaluated from the Lagrangian formalism or be defined in an effective way to fully recover the electronic energy.[13–16] Moreover, two IQA partitions consistent with density functional theory that involve the explicit integration of the exchange-correlation kernel over the atomic regions have been proposed.[17,18] Additionally, the formalism to perform the partition in excited states with the EOM-CCSD method has been recently introduced.[7] Nevertheless, of these electronic structure methods in which the IQA decomposition has been implemented, none is flexible enough or provides sufficient accuracy to tackle processes that needs a multi-configurational description; for example, bond breaking or the crossing of electronic states of the same spin multiplicity.

There are applications of the IQA partition with the CASSCF and the MRCI-SD methods,[11,12] although the lack of dynamic correlation in the former and the high computational scalability cost of the latter limit the range of systems that can be studied. For example, for most of organic molecules with medium size choices of active spaces CASSCF leads to considerable errors in the calculation of the vertical transition energies,[19] and in addition, it may predict an incorrect ordering of the nature of the electronic states, which may ultimately

result in providing an incorrect picture of the photochemical mechanism.

In the present work we show how to perform the IQA partition consistent with second order perturbation theory with a complete active space self-consistent field reference function (CASPT2).[20] The CASPT2 method presents a good balance between cost-effective and accurate determination of approximate solutions to an electronic structure problem regardless the molecule or process under study. Despite not being a black box, its versatility has led it to be one of the most popular multiconfigurational methods used for the study of processes of photochemical relevance, for example, the sub-picosecond ultra-rapid decay of DNA bases.[21,22] Also, efficient CASPT2 implementations have greatly extended the applicability to molecules with more than 100 atoms, as well as the use of active spaces above (20e,20o) in the present days.[23–25] Given the flexibility of CASPT2 for the accurate description of the electronic structure of molecules, the IQA/CASPT2 decomposition is particularly relevant as a model for rationalizing the energy changes involved in processes that take place in excited states.

The structure of the article is as follows. First, a brief description of the IQA energy partition is given. Later, the CASPT2 effective density matrices necessary to carry out the energy decomposition are presented. Subsequently, the application of the CASPT2 based IQA approach for representative processes that span different bonding regimes are provided: the formation of noble gas excimers and exciplexes, the reaction between Cl and O_3 and the photodissociation of formaldehyde and cyclobutane. The purpose of using CASPT2 with these systems is to perform a quantitative description as well as to analyze representative excited state processes. For selected cases, it is also analyzed how the trends in the energetic analysis change with the inclusion of the dynamic correlation, when going from the CASSCF description to CASPT2. Finally, the main conclusions are presented.

Methods

IQA energy decomposition

The IQA approach performs an exact decomposition of the molecular electronic energy based only on physical, well-defined contributions which have an immediate chemical reading. Its only tenet is the identification of regions of space with atoms, typically through the Quantum Theory of Atoms in Molecules.[26] Since the spatial partition is exhaustive, e.g. the union of all the atomic regions or basins fills the space, once these regions are defined the expectation values of one- and two-electron operators become the sum of one- and two-center, intra- and interatomic components, respectively. In keeping with the tradition in atomistic simulations, all the intra-atomic terms related to an atom A are gathered to build the so-called atomic self-energy, while all the interatomic ones pertaining to a given atomic pair A, B are identified with their mutual interaction energy:

$$E = \sum_{\mathrm{A}} E^{\mathrm{A}}_{self} + \frac{1}{2} \sum_{A} \sum_{\mathrm{B} \neq \mathrm{A}} E^{\mathrm{A,B}}_{int} \tag{1}$$

Detailed expressions of how to carry out this procedure have been presented elsewhere.[2,27] The self-energy of atom A, E^{A}_{self} involves the sum of the kinetic energy of all electrons residing in A, T^{A}, their electrostatic attraction to nucleus A, $V^{\mathrm{A,A}}_{en}$, and their mutual electron-electron repulsion, $V^{\mathrm{A,A}}_{ee}$. The latter can be partitioned into a Coulomb repulsion term, which is profitably added to $V^{\mathrm{A,A}}_{en}$ to form the total intra-atomic electrostatic energy, V^{A}_{ele}, and the quantum-mechanical correction to it, the intra-atomic exchange-correlation energy, V^{A}_{xc}:

$$E^{\mathrm{A}}_{self} = T^{\mathrm{A}} + V^{\mathrm{A}}_{ele} + V^{\mathrm{A}}_{xc} \tag{2}$$

Similarly, the interaction energy between atoms A and B is made up of electrons of A with nucleus of B and nucleus of A with electrons of B attractions, $V^{\mathrm{A,B}}_{en}$ and $V^{\mathrm{A,B}}_{ne}$, intercenter electron repulsion, $V^{\mathrm{A,B}}_{ee}$, and nucleus-nucleus repulsions, $V^{\mathrm{A,B}}_{nn}$. If we now decompose $V^{\mathrm{A,B}}_{ee}$

into a Coulomb contribution and an exchange-correlation one, and gather all the terms but $V_{xc}^{\mathrm{A,B}}$ into an electrostatic interaction, V_{ele}^{A},

$$E_{int}^{\mathrm{A,B}} = V_{ele}^{\mathrm{A,B}} + V_{xc}^{\mathrm{A,B}} \tag{3}$$

Several reasons explain the success of the IQA decomposition. First, its asymptotic properties are physically sound, for at large interatomic separations, E_{self}^{A} tends to the free atomic energy, and $E_{int}^{\mathrm{A,B}}$ to the standard perturbation theory interatomic energy. Second, it can be applied for a wide range of theoretical levels, at any molecular geometry, be it a stationary one or not, and equally for ground and excited states. Third, the union of several atoms to form interacting fragments or molecules is straightforward, so self-energies as well as interaction energies are available at any level of coarse-graining, from the atom up to the full system. Moreover, The lion's part of the total molecular energy is isolated in the self-energy terms. This means that, for chemical purposes, where only energy changes are truly relevant, large quasi-constant terms can be safely ignored. It is then convenient to introduce an atomic (or fragment) deformation energy, E_{def}^{A} defined as the difference between E_{self}^{A} and a reference energy value for the reference, for instance the same self-energy at a well-defined dissociation limit. For example, for a diatomic molecule A-B the deformation energy of atom A can be defined as

$$E_{def}^{\mathrm{A}}(R) = E_{self}^{\mathrm{A}}(R) - E_{self}^{\mathrm{A}}(R = \infty) \tag{4}$$

E_{def}^{A} and E_{def}^{B} account for the intra-atomic redistributions that take place upon bond formation, vanishing when no fragment interacts with any other. This implies that all E_{def}^{A}, E_{def}^{B} and $E_{int}^{\mathrm{A,B}}$ have usually the same order of magnitude as the binding energy ($E_{bind} = E_{def}^{\mathrm{A}} + E_{def}^{\mathrm{B}} + E_{int}^{\mathrm{A,B}}$), thus facilitating the interpretation of a process. Similarly, in the study of an intrinsic reaction coordinate it is possible to refer the E_{self}^{A} and $E_{int}^{\mathrm{A,B}}$ values to a particular geometry (e.g. the reactants at infinite separation). The change of energy along the

process, ΔE, is then

$$\Delta E = \sum_{A} E^{\mathrm{A}}_{def} + \frac{1}{2} \sum_{A} \sum_{\mathrm{B} \neq \mathrm{A}} \Delta E^{\mathrm{A,B}}_{int} \tag{5}$$

making it possible to analyze the atomic and pairwise contributions to the total energy changes for a given process. Finally, it is particularly satisfying that all the energy contributions in IQA bear a clear chemical counterpart. Deformation energies measure promotion from the chemically relevant reference, and thus quantify steric hindrance.[28] The interatomic electrostatic energy and its exchange-correlation counterparts are direct measures of the ionic and covalent components of a given interaction, respectively. Interestingly, they admit Taylor expansions with leading terms inversely proportional to the interatomic distance, that scale with the product of the atomic charges in the case of $V^{\mathrm{A,B}}_{ele}$ (Coulomb's law for ionic behavior) and with the bond order when $V^{\mathrm{A,B}}_{xc}$ is considered.[29]

CASPT2 effective density matrices

For a variational method, the electronic energy of a molecular system described by a normalized wavefunction $|\Psi\rangle$ is given by[30]

$$E = \langle \Psi | \hat{H} | \Psi \rangle = \sum_{pq} D_{pq} h_{pq} + \frac{1}{2} \sum_{pqrs} d_{pqrs} g_{pqrs} \tag{6}$$

where h_{pq} and g_{pqrs} are the mono and bielectronic integrals in the molecular orbital basis and D_{pq} and d_{pqrs} are elements of the first and second order density matrices. The latter can be obtained from the expectation value of the one and two particle excitation operators over $|\Psi\rangle$ expressed as linear combinations of determinants ($|\psi_i\rangle$)

$$D_{pq} = \langle \Psi | \hat{E}_{pq} | \Psi \rangle = \sum_{\sigma=\{\alpha,\beta\}} \sum_{i,j} c_i c_j \, \langle \psi_j | a^{\dagger}_{p\sigma} a_{q\sigma} | \psi_i \rangle \tag{7}$$

$$d_{pqrs} = \langle \Psi | \hat{e}_{pqrs} | \Psi \rangle = \sum_{i,j} c_i c_j \, \langle \psi_j | \hat{E}_{pq} \hat{E}_{rs} - \delta_{qr} \hat{E}_{ps} | \psi_i \rangle \tag{8}$$

which involve the product of the CI vector with the one $\gamma^{ji}_{pq} = \sum_{\sigma=\{\alpha,\beta\}} \langle\psi_j|a^\dagger_{p\sigma}a_{q\sigma}|\psi_i\rangle$ and two-electron $\Gamma^{ji}_{pqrs} = \langle\psi_j|\hat{E}_{pq}\hat{E}_{rs} - \delta_{qr}\hat{E}_{ps}|\psi_i\rangle$ coupling coefficients. The starting point of the IQA method corresponds to the right-hand side of (6), which makes the need to obtain the density matrices evident. For the CCSD and MP2 methods, it is possible to rewrite the respective energetic expressions in the same form as in (6).[13–16] However, in these cases D_{pq} and d_{pqrs} are not obtained as in (7) or (8) and therefore are termed "effective density matrices".

The former approach can be extended to CASPT2, a method that uses second order Rayleigh-Schrödinger perturbation theory, on top of a CASSCF wavefunction, in order to recover a major part of the correlation energy.[20] The flexibility of including a multiconfigurational reference function allows to describe situations such as bond breaking, excited states, spin coupling processes, and in some cases, avoided crossings and conical intersections.[31] Briefly, the CASPT2 energy for a specific electronic state of an atomic or molecular system is given by[32]

$$E = \langle\Psi^0|\hat{H}|\Psi^0\rangle + \langle\Psi^0|\hat{H}|\Psi^1\rangle + \langle\Psi^1|\hat{H}|\Psi^0\rangle + \langle\Psi^1|\hat{H}^0 - E^0|\Psi^1\rangle \tag{9}$$

where $|\Psi^0\rangle$ and $|\Psi^1\rangle$ respectively are the CASSCF reference and the first order perturbative correction to the wavefunction. In addition, $E^n_0 = \langle\Psi^0|\hat{H}^0|\Psi^0\rangle$, $\hat{H}^0$ being an effective one electron operator

$$\begin{aligned}
\hat{H}^0 &= \hat{P}\hat{f}\hat{P} + \hat{Q}\hat{f}\hat{Q} \\
\hat{f} &= \sum_{pq} f_{pq}\hat{E}_{pq} \\
f_{pq} &= h_{pq} + \sum_{rs} D^{0,0}_{pq}(g_{pqrs} - \frac{1}{2}g_{prqs})
\end{aligned} \tag{10}$$

whereas $\hat{P} = |0\rangle\langle 0|$ and $\hat{Q} = 1 - \hat{P}$ are projectors onto the CASSCF wave function and its orthogonal complement. Note that the CASSCF one electron density matrix ($D^{0,0}_{pq}$) is involved

in f_{pq}. Introducing the explicit definitions of $\hat{H}^0$ and $\hat{H}$, taking into account the permutational symmetry of g_{pqrs} and grouping the result in mono and bielectronic contributions, it is possible to rewrite (9) as

$$E = \sum_{pq} D'_{pq} h_{pq} + \frac{1}{2} \sum_{pqrs} d'_{pqrs} g_{pqrs} \tag{11}$$

Let M and N be 0 or 1 so that $|\Psi^M\rangle$ or $|\Psi^N\rangle$ correspond to the reference function or to the first-order correction. Using the notation

$$D^{M,N}_{pq} = \langle \Psi^M | \hat{E}_{pq} | \Psi^N \rangle$$
$$d^{M,N}_{pqrs} = \langle \Psi^M | \hat{e}_{pqrs} | \Psi^N \rangle$$

D'_{pq} and d'_{pqrs} are obtained as

$$D'_{pq} = (1 - \langle \Psi^1 | \Psi^1 \rangle) D^{0,0}_{pq} + D^{1,1}_{pq} + D^{1,0}_{pq} + D^{0,1}_{pq} \tag{12}$$

$$\begin{aligned} d'_{pqrs} = {} & d^{0,0}_{pqrs} + d^{0,1}_{pqrs} + d^{1,0}_{pqrs} + 2 D^{0,0}_{rs} D^{1,1}_{pq} \\ & - D^{0,0}_{qs} D^{1,1}_{pr} - 2 \langle \Psi^1 | \Psi^1 \rangle D^{0,0}_{rs} D^{0,0}_{pq} + \langle \Psi^1 | \Psi^1 \rangle D^{0,0}_{qs} D^{0,0}_{pr} \end{aligned} \tag{13}$$

Similar expressions to (12) and (13) have been defined in the context of analytical gradient theory for CASPT2.[32] It should be stressed that (11) has the same functional form as (6), where D'_{pq} and d'_{pqrs} play the role of effective one- and two-electron density matrices. As long as D'_{pq} and d'_{pqrs} are used together with the molecular orbital information in which they are expressed, the IQA implementation here proposed fully recovers the electronic energy; notwithstanding, these matrices are not suitable for the evaluation of other properties. In contrast to the MP2 method,[16] CASPT2 induces changes on the CASSCF first-order density; it affects all the contributions to E_{self} and E_{int}, not only the V_{xc} term.

The inclusion of a level shift is often resorted to in order to achieve convergence of the CASPT2 procedure or to avoid the presence of intruder states;[33,34] however, the level-shift

corrected energy is equivalent to evaluating the final Hylleraas functional (eq. 9) without the shift. Also, for some excited state calculations convergence problems in the perturbative expansion arise that are removed when replacing $D^{0,0}_{pq}$ in (10) with the CASSCF state-averaged density matrix.

The above definitions for D'_{pq} and d'_{pqrs} are the starting points to apply the IQA partitioning to the multistate variants of CASPT2. Single state CASPT2 (used in the present work) employs a generalized Fock operator that is not diagonal on the $|\Psi^0\rangle$ basis and depends on the density matrix of only one of the CASSCF roots. On the other hand, for the MS-CASPT2[35] or XMS-CASPT2[36] variants, the operator $\hat{f}$ depends on more than one reference state. Moreover, for the latter the electronic energies are obtained from the diagonalization of an effective Hamiltonian $\mathbf{H}_{eff}$, whose diagonal elements correspond to equation (9), and the non-diagonal parts involve the coupling of the perturbative corrections and CASSCF wavefunctions of different states. Once $\mathbf{H}_{eff}$ is diagonalized, the effective perturbative correction in MS-CASPT2 and XMS-CASPT2 would correspond to a linear combination of the SS-CASPT2, and therefore, the respective multistate density matrices would be obtained from a linear combination of D'_{pq}, d'_{pqrs} and transition density matrices. Since the above process is elaborate and computationally involved, it deserves further exploration in a separate study.

Computational details

The electronic structure calculations were carried out without symmetry restrictions at the CASPT2 level and using a level shift of 0.3 a.u. with the Molpro and Bagel programs.[37–39] In all the cases, the orbitals of the CASSCF reference wave functions were optimized using equal weights in the state average process. The aug-cc-pVDZ basis set was employed for the noble gases calculations, adzp was used for Xe_2 and def2-sv(p) for the rest of systems.[40–42] The active spaces comprise the following (number of electrons, number of orbitals) pairs: He_2

(2e,5o), HeNe (4e,10o), noble gases excimers (4e,5o), noble gases exciplexes (7e,4o), H_2CO (12e,10o), O_3 + Cl (9e,7o) and C_4H_8 (4e,5o). For the noble gases excimers, a molecular orbital with almost zero occupation for all internuclear distances was included in the active space. This has minor consequences on the potential energy curves, but induces a symmetry breaking that allows to distinguish between ground or excited atoms at the dissociation limit. Notice then, that the presentation here differs from the symmetry preserving one discussed in a previous reference.[11] For the cyclobutane, two σ, two $\sigma^\star$ and one Rydberg orbitals were included in the active space for the proper description of the S_1 state.[43]

For the evaluation of (12) and (13), the first order perturbative correction to the wavefunction was first expressed as a linear combination of determinants. Detailed information about this procedure can be found in a previous work for the use MRCI-SD wave functions with the IQA method,[11] which uses the same contraction scheme as CASPT2 (as implemented in Molpro) for single and double excitations. This step was performed in order to facilitate the evaluation of the coupling coefficients;[44] for example, γ^{ji}_{pq} only depends on the occupation pattern of the determinants and has integers values, whereas if contracted bielectronic or configuration state functions are used its evaluation becomes more complicated. To obtain the CASPT2 effective density matrices, a fortran program that processes the wave function information provided by Molpro was implemented. It computes the coupling coefficients and the involved operations. The partitioning of the total energy by the IQA method was carried out with the Promolden program.[45]

Results and discussion

Excimer and exciplex formation

The formation of excimers and exciplexes play a central role in many photochemical processes, ranging from DNA damage to light harvesting.[46] Rare gas (Rg) complexes are used as laser active media in the UV region, which have diverse applications in lithography, food

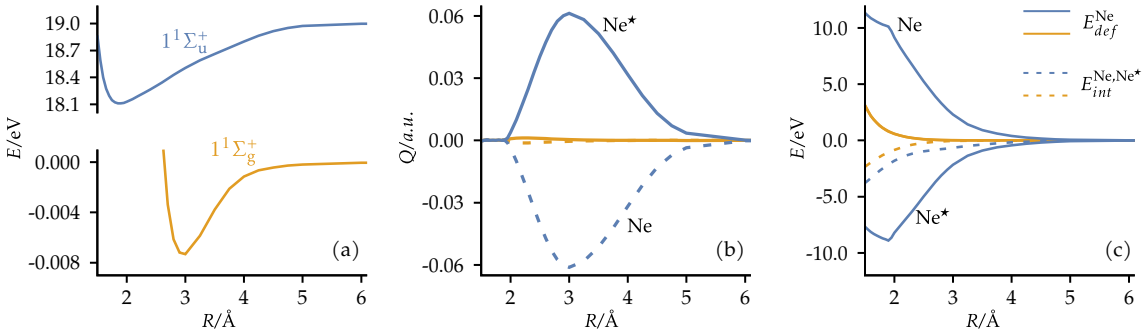

Figure 1: (a) Potential energy curves for the electronic $1^1\Sigma_g^+$ (yellow) and $1^1\Sigma_u^+$ (blue) states of Ne_2. (b) Atomic charges and (c) IQA energetic components as a function of the internuclear distance. Ne* denotes the excited atom at the dissociation limit.

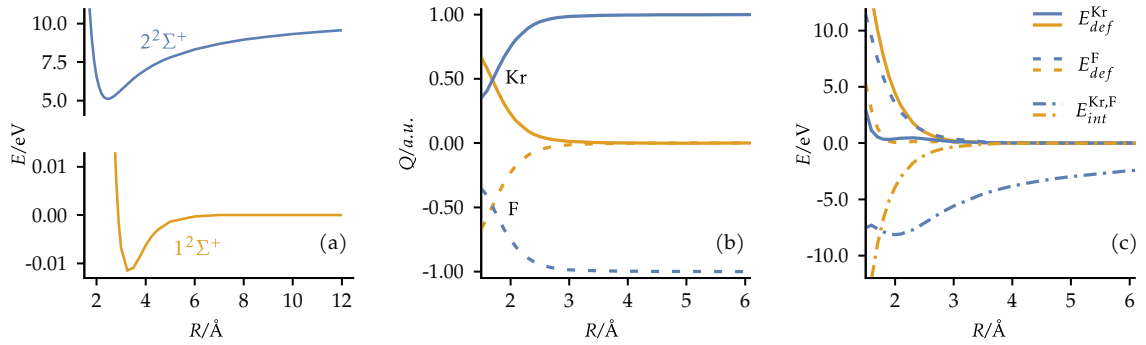

Figure 2: (a) Potential energy curves for the electronic $1^2\Sigma^+$ (yellow) and $2^2\Sigma^+$ (blue) states of KrF. (b) Atomic charges and (c) IQA energetic components as a function of the internuclear distance.

processing and medicine.[47–49] Despite its apparent structural simplicity, the time resolved experimental characterization of Rg_2 excited complexes requires elaborate arrangements, particularly because of the short wavelengths involved.[50,51] From the theoretical point of view, several chemical bonding models have been used for their description. For example, Birks and others proposed that bonding in excimers arises from a configurational mixing between excited and charge transfer states.[52,53] However, these ideas are rooted on long-range excitonic models (e.g., Frenkel-Davydov), which do not apply to the short internuclear distances observed at the equilibrium geometry. In this regard, the use of the IQA decomposition scheme can be useful to rationalize the nature of the interactions on these complexes over the entire range of distances; importantly, without introducing additional approximations to those already implicit in the evaluation of electronic energies. In brief, the IQA

decomposition is able to explain what are the energetic contributions that give rise to the formation of the Rg_2 and RgF intermolecular complexes in the excited state. The use of CASPT2 is not obligatory for a qualitative description of these systems, but it is useful to obtain a quantitative energetic agreement, comparable with experimental results. This methodology has been previously applied to the case of He_2 in the singlet and triplet ground and lowest excited states using MRCI-SD wavefunctions.[11]

The first step involved in the excimer formation process is an excitation of the Rg atom to the first excited singlet state. The vertical absorption energies range from 21.45 eV for He to 9.59 eV for Xe at the present level of calculation. For He, the transition is prohibited by the Laporte rule (zero oscillator strength), whereas in the other atoms the intensity increases throughout the series. Once the noble gas is at the 1^1P_1 (or 2^1S_0 for He_2) state its interaction with a second Rg atom in the ground state leads to the formation of two possible singlet states associated with the even ($2^1\Sigma_g^+$) and odd ($1^1\Sigma_u^+$) combinations of the atomic wavefunctions. Table S1 presents a summary of the energetic and structural parameters of all the studied complexes, as well as their comparison with experimental data and from other theoretical studies; overall, a good agreement is observed, except for specific data. In some circumstances, the origin of these discrepancies can be explained. For example, the experimental assignment for the $1^1\Sigma_u^+ \rightarrow 1^1\Sigma_g^+$ transition of He_2 is not entirely clear, due to the appearance of a continuum. Also, for the systems containing Xe, the inclusion of relativistic effects and extended basis sets are required for the proper description of the PES.[54,55] An increase of the base size also improves the description of the parameters of table S1, but in general, the evolution of the IQA components as well as the underlying interpretation remain the same (fig. S1).

Figure 1(a) presents the potential energy curves for the two lowest singlet electronic states of Ne_2. The binding energy (E_{bind}) of $1^1\Sigma_g^+$ is of 0.007 eV, which reflects the near-zero interaction between two Ne(1^1S_0) atoms, in agreement with the chemical intuition. The almost zero deformation energies over all the range of internuclear distances (R) are consistent with

the small E_{bind} value, i.e., show that the electronic distribution of the Ne atoms remains practically unchanged. Only the slight decrease of $E_{int}^{\mathrm{Ne,Ne^\star}}$ near 2.97 Å accounts for the formation of this weak intermolecular complex. The behavior of $1^1\Sigma_u^+$ contrasts significantly to the ground state. For example, at the initial stage of excimer formation (from 5 to 3 Å) there is a charge transfer of up to 0.06 e from the excited neon atom ($Ne^\star$) which is subsequently reversed giving rise to a neutral complex at ca. 2 Å, Fig. 1(b). This shows that in this region the configurational mixing with a charge transfer state is not negligible. Although it is not explicitly analyzed, it has been previously shown that this behavior occurs where a change in the nature of the electronic state is involved.[11] Concomitant to the charge transfer, there is a considerable decrease in the deformation energy of $Ne^\star$, with an increase for the ground state atom, Fig. 1(c), that can be interpreted as an energy flow from the excited to the ground state Ne.

A detailed analysis of the self-atomic components reveals that the largest changes take place on the electrostatic contributions in both atoms (Fig. S2a). Near the equilibrium geometry the atomic self-energies are almost equal, thus precluding to distinguish the Ne atoms (Fig. S2b). Regarding the interaction term, $V_{xc}^{\mathrm{Ne,Ne^\star}}$ is the largest contribution to $E_{int}^{\mathrm{Ne,Ne^\star}}$ for $R < 8$ Å; $V_{ele}^{\mathrm{Ne,Ne^\star}}$ is only relevant when the charge transfer takes place and is positive for $R < 2$ Å (Fig. S2c). The trends in E_{def}^{Ne} and $E_{int}^{\mathrm{Ne,Ne^\star}}$ suggest that the excimer association mechanism can be perceived as the formation of a conventional chemical bond, similar to the ground state of an heterodiatomic AB molecule.[56] That is, in both cases a significant change take place in the internal electronic structure of atoms A and B with a destabilizing effect (measured by E_{def}), but which is more than compensated by and reinforcement of their mutual interaction $E_{int}^{\mathrm{A,B}}$, mainly due to the covalent term.

In summary, the observed value of 0.889 eV for the binding energy of the $1^1\Sigma_u^+$ state in Ne_2 arises as a combination of two effects: 1) the energy transfer from $Ne^\star$ to Ne, that makes a destabilizing contribution to the total system (negative contribution to E_{bind}) and 2) the Ne-Ne covalent interaction that dominates $E_{int}^{\mathrm{Ne,Ne'}}$. Note how all this quantitative

information about the mechanism of excimer formation is implicit in the electronic energies, but the analysis focused only on the PES is not able to reveal. In line with Birks model, the IQA decomposition provides evidence that configurational mixing with charge transfer states $Rg^- - Rg^+ \leftrightarrow Rg^+ - Rg^-$, although not negligible, is not relevant for the quantitative description of the Rg_2 excited complexes. The data are more consistent with what is called excitonic resonance $Rg - Rg^\star \leftrightarrow Rg^\star - Rg$, which can be perceived as a delocalization of the excitation energy. Figures S3 and S4 report the potential energy curves and the IQA decomposition for HeNe and others Rg_2 excited state complexes. Although charge and energy transfer decrease throughout the series, the changes of the components as a function of the internuclear distance are very similar to those of Ne_2, which suggests that the excimer formation mechanism of rare gases is generic. That is, the process can be described as a energy transfer from $Rg^\star$ to Rg that enhances the interaction between the Rg-$Rg^\star$ fragments, again, consistent with excitonic resonance.

Noble gases also form charge transfer compounds with halogens by the interaction between two ionic fragments. For example, in case of the KrF molecule, the difference between the ionization potential of Kr and the electronic affinity of F is 10.68 eV at the present level of calculation. This value is lower than the energy associated with the first singlet transition of Kr (12.16 eV) or the doublet of F (14.49 eV). Therefore, the $2^2\Sigma^+$ state of KrF dissociates to $Kr^+ + F^-$ (fig. 2a). Charge transfer states are also present for ArF, NeF and HeF, but have higher energies than their lower Rydberg excited states.

The behavior of the ground state of KrF is very similar to the $1^1\Sigma_g^+$ for Ne_2, as the Kr and F moieties can be considered as weakly interacting based on the small observed values for E_{bind}, E_{def}^{Kr}, E_{def}^{F} and E_{int}. However, $V_{ele}^{\mathrm{Rg,F}}$ is the most important contribution to the binding energies of the charge transfer complexes ($2^2\Sigma^+$), even at large internuclear distances as evidenced by the value $E_{int}^{\mathrm{Kr,F}} = -2.45$ eV at 6.0 Å (fig. 2c). At the equilibrium geometry, the $V_{xc}^{\mathrm{Rg,F}}$ values are stabilizing, ranging from -0.84 eV for NeF to -1.48 eV in XeF, indicating that the covalent component of $E_{int}^{\mathrm{Rg,F}}$ is also a relevant bonding contribution.

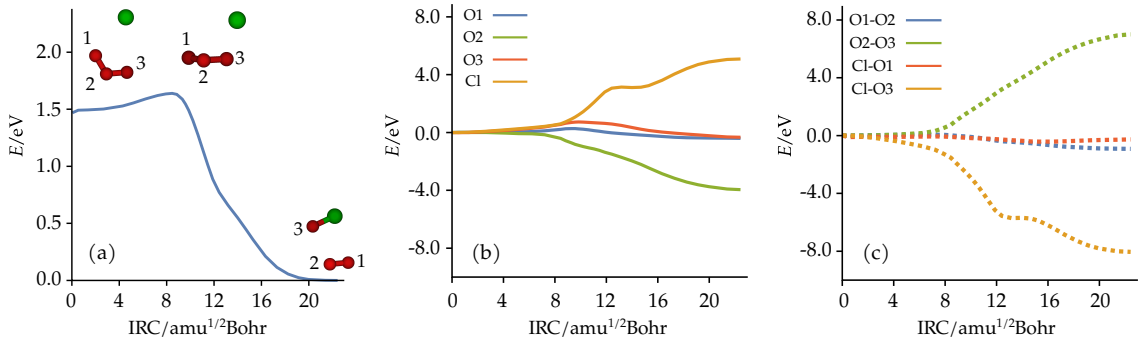

Figure 3: (a) Total energy throughout the IRC of the O_3+Cl $\rightarrow$ O_2+ClO reaction. The main structures are shown over the regions. (b) Self-atomic and (c) inter atomic energy contributions relative to their values at the beginning of the reaction. Labelling of the O atoms is shown in (a).

Also, unlike to the Ne_2 excimer where changes in E_{def} for Ne and Ne* show opposite trends, for the $2^2\Sigma^+$ state of KrF the E^{F}_{def} value increase considerably while E^{Kr}_{def} remains constant upon the approaching of the fragments. Therefore, a transfer of energy between Kr and F cannot be considered to take place. In terms of the IQA data and the Birks model, the $2^2\Sigma^+$ states of the RgF complexes can be categorized as charge transfer in nature, i.e. pure $\mathrm{Rg}^+ - F^-$, where surprisingly the exchange-correlation interaction term makes a significant contribution to E_{bind}. Furthermore, given the asymptotic limit RgF $\rightarrow$ $\mathrm{Rg}^+ + \mathrm{F}^-$ and the long-range behavior shown in $V^{\mathrm{Rg,F}}_{ele}$, it is evident that the electrostatic component is the driving force for the formation of these compounds (Figs. S5 and S6).

O_3+Cl reaction

The reaction of O_3 with a chlorine atom, released by the photolysis of chlorofluorocarbons,

$$\mathrm{O_3 + Cl \longrightarrow ClO + O_2}, \tag{14}$$

is very important in the chemistry of the stratosphere[57,58] because of the role ClO plays in the catalytic ozone depletion cycle. For instance, the ClO fragments can lead to the formation of chlorine peroxide, which can dissociate by photolysis to give rise to O_2 and

more Cl radicals. The multiconfigurational nature of process (14) is well documented,[59] making the use of methods such as CASPT2 necessary to satisfactorily describe the intrinsic reaction coordinate (IRC), as the barrier is highly overestimated and the reaction energy is underestimated without accounting for the dynamical correlation. It has been shown that the reaction of O_3 (X^1A_1) with Cl (^2P) proceeds as a doublet for the total system on a PES well separated from other electronic states and without nonadiabatic or spin-flip transitions.[59] In addition, the reaction takes place without intermediates and is highly exergonic (Fig. 3a), with a reaction energy of -1.47 eV and a low energy barrier of 0.17 eV at the present level of calculation.

The IQA decomposition enables a detailed and concise description of the process (14) along the IRC. Mainly, it allows to identify the atomic and pair contributions to the involved energy barrier, and also, the terms that globally drive the chemical reaction. In this way, it is possible to conceptualize the transformation in (14) as an energy balance, taking into account separately the atomic terms, as well as the breaking and/or formation of the involved bonds. This type of information is of importance for rationalizing reactions between radicals in an atomic view, contrary to the usual analysis of the relevant electronic configurations in the orbital basis, where interpretation is difficult due to the highly multiconfigurational nature of the system. The initial approach between the O_3 and Cl fragments is driven by the O3-Cl interaction, but this results in a distortion on the electronic structure of O1, O3 and Cl with a consequent increase in E_{def}^{O1}, E_{def}^{O3} and E_{def}^{Cl}, as well as a weakening of the O2-O3 interaction. This can be seen from the analysis of the IQA contributions between 0 and 8 amu$^{1/2}$Bohr (fig. 3), which shows that the energy barrier appears because of an increase of the atomic terms (except for the O2 atom) and of the $E_{int}^{\mathrm{O2,O3}}$ component.

Once the barrier is surpassed, $E_{int}^{\mathrm{O2,O3}}$ continues to increase and $E_{int}^{\mathrm{Cl,O3}}$ decreases almost monotonically signaling the concerted O2-O3 bond breaking and Cl-O3 bond formation. In addition, the self-energies of O1 and O2 evolve to their corresponding values in the O_2 molecule. Fig. 3 also shows that E_{self}^{Cl} and $E_{inter}^{\mathrm{Cl,O3}}$ exhibit a plateau between c.a. 12 and 16

amu$^{1/2}$ Bohr, despite the large changes occurring in the orientation of Cl with respect to O_3 and in the Cl-O3 distance. This behavior is in line with the trends of atomic charges and the V_{xc} contribution to the self- and interaction components of the atoms involved (Fig. S7). The IQA analysis shows that the concerted reaction is accompanied by the stabilization of O2 and destabilization of Cl along the process ($E_{def}^{O2} + E_{def}^{Cl} > 0$), which is more than compensated by the increase in the magnitude of the O3-Cl interaction.

Photodissociation of H_2CO

The α-cleavage of ketones is one of the best known and most important reactions driven by light absorption.[60] In particular, there is an enormous body of theoretical and experimental information for the decomposition of formaldehyde following the initial excitation to the S_1 ($^1n\pi^\star$) state, including the study of the time-resolved dynamics and the full exploration of the respective potential energy surfaces.[61–65] At low-photon energies the main dissociation channels of H_2CO are

$$H_2CO \longrightarrow HCO\cdot + H\cdot \tag{15}$$

$$H_2CO \longrightarrow CO + H_2 \tag{16}$$

where the α-cleavage, proceeding through radicals species, has the lowest energy barrier on the S_1 surface. Additionally, due to the small singlet-triplet energy gap and in agreement with the El-Sayed rules[66] the intersystem crossing is favored, so the above processes also take place on the T_1 ($^3\pi\pi^\star$) manifold. The IQA decomposition (at the CASSCF level) and real-space focused models have previously been used in order to rationalize the photochemical relaxation of H_2CO towards the minimum of the $^1n\pi^\star$ state.[12] In the present work, we extend this endeavor by considering the minimum energy path (MEP) of $^1n\pi^\star$ state for the α-cleavage, starting at the Franck-Condon region and ending with an accessible conical intersection with S_0. Additionally, we analyze the MEP for $^1n\pi^\star$ proceeding through the lowest S_1/T_1 minimum energy crossing point (MECP) and finishing with the molecular

elimination depicted in (16), which for the $^3\pi\pi^\star$ state involves a lower barrier than (15). The objective is to quantify in a mechanistic approach the energetic changes involved in the surface crossing, that are relevant to rationalize the internal conversion and the intersystem crossing processes.

The first step on the photochemistry of H_2CO is the electronic $S_0 \rightarrow S_1$ transition, whose optical gap is of 3.80 eV at the CASPT2 level. Figure 4 presents the changes on the atomic and interaction components between the S_0 and $^1n\pi^\star$ states, making possible to dissect the vertical transition energies in order to quantify the contribution of each atom and pair. In summary, the changes on self-energies are negative for the carbon and oxygen atoms and positive for the respective pair term ($E_{int}^{C,O}$). Regarding the origin of the atomic stabilization, a detailed analysis shows that after the electronic transition, the atomic population of C increases while that of O decreases, so that the nucleus-electron attraction becomes more negative in C and the electronic repulsion decreases in O, thus explaining the changes in both E_{self}^{C} and E_{self}^{O}. On the other hand, this population transfer is reflected in a stronger electron-electron repulsion between the C and O atoms, thus clarifying the weakening of the C=O interaction ($\Delta E_{int}^{C,O} > 0$).

The data at the CASSCF level are also included in Fig. 4, making it possible to compare the effect of the dynamic correlation on the changes of the IQA energies. A detailed analysis of the effect of active space size on the energetic changes of these atomic and pair contributions is presented in the supporting information (fig. S8). To summarize, the energy trends are similar, but the relative contribution of each component can change significantly. The latter is particularly relevant for the choice of minimum active spaces. In fact, the changes in the contributions evaluated with CASSCF appear to converge to CASPT2 values as the size of the active space increases. As it can be seen from the data of fig. 4, which involves the full valence orbitals in the active space, the correlation energy is not localized in an atomic or interaction part, and in general, the magnitude of the CASSCF terms are slightly greater than those using CASPT2.

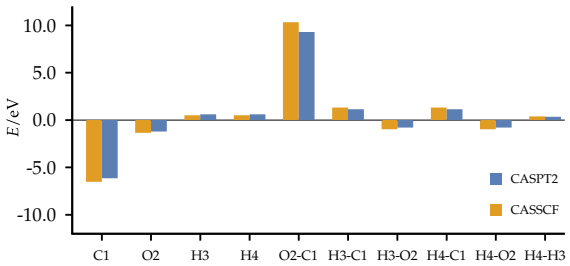

Figure 4: Differences in self-energies and interaction terms between the S_0 and $^1n\pi^\star$ states of H_2CO at the equilibrium geometry of S_0. The absorption energy is of 3.80 eV for caspt2 and 4.14 eV for CASSCF, using in both cases an active space of (12e,10o). The experimental estimate ranges from 3.79 to 4.07 eV.[67,68]

The MEP for the α-cleavage proceeding in the $^1n\pi^\star$ state can be split for convenience into four regions (Fig. 5a), which account for important structural or energetic changes.[64] The first zone goes up to 0.5 amu$^{1/2}$Bohr and involves the elongation of the C=O bond, whereas region II goes from 0.5 to 2 amu$^{1/2}$Bohr where the pyramidalization of the carbon atom bonding pattern occurs. Subsequently, the third zone covers from the energy minimum to the transition state. Finally, in zone IV the crossing between the electronic states takes place.

In region I there is a considerable decrease of E^{C}_{self} and E^{O}_{self}, accompanied by an increase of $E^{\mathrm{C,O}}_{int}$ (fig. 5) on the $^1n\pi^\star$ state, involving an stabilization of the carbon and oxygen atoms and a further weakening of the C=O interaction with regard to the structure at the Franck-Condon region. For carbon, this is mainly due to a more negative V^{C}_{en} term, while in the oxygen there is a decrease in the kinetic energy. In the pair term, the origin can be traced to $V^{\mathrm{C,O}}_{ele}$ and $V^{\mathrm{C,O}}_{xc}$, with a larger contribution from the former. These trends are in line with a change in the hybridization from sp^2 to sp^3 for the C atom, as well as a change on nature of the C-O contact from double to single bond.[12] The energetic modifications that take place in region I pave the way for the pyramidalization of the C atom in region II, where minor energetic changes are observed. The transition state is 1.13 eV higher than the energy minimum. The changes for E^{C}_{self}, E^{O}_{self} and $E^{\mathrm{C,O}}_{int}$ in region III are in the reverse direction to those occurring in I and II, suggesting that in order to access the transition state, and

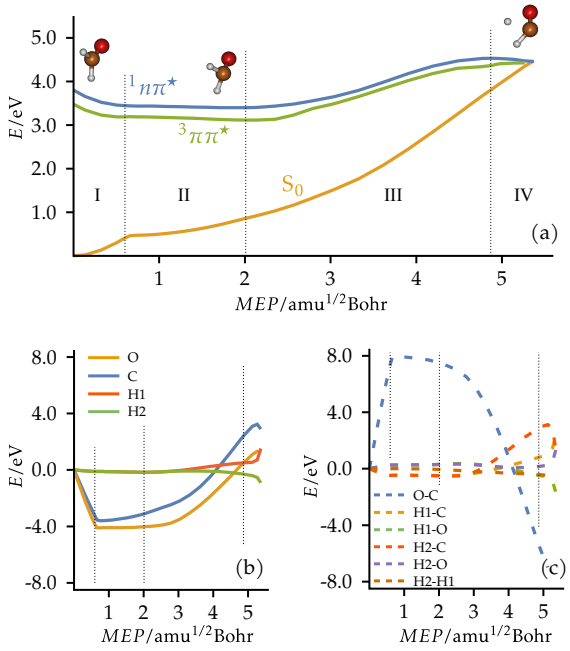

Figure 5: a) Energies of the low-lying states of H_2CO along the minimum energy path (MEP) of $^1n\pi^\star$. Changes on the b) self-energies and c) Interaction terms for the $^1n\pi^\star$ state along the MEP. The data in b and c take as reference the value at the starting point.

thereby approach the S_1/S_0 intersection seam, an sp^2 rehybridization of the carbon atom is necessary, in agreement with the formation of the formyl radical. As in Figure 4, single-point IQA/CASSCF calculations along the MEP evaluated with CASPT2 provide the same information about the mechanism (fig. S9), however, the height of the barrier to access the conical intersection is highly underestimated, so a more quantitative picture is obtained using the CASPT2 approach. Nevertheless, this suggest that when differential correlation effects are not important the cheaper IQA/CASSCF energies can be used for rationalization of the mechanism.

Interestingly, at the conical intersection one of the C-H distances is 1.689 Å, but the analysis of the molecular graphs for S_0 and S_1 reveals the occurrence of a bond-critical point between the respective atoms. Also, the associated $E_{int}^{C,H}$ term for the S_1 state has a stabilizing contribution of -3.63 eV (-0.77 eV for S_0). Moreover, the topological analysis for the Laplacian of the electron density reveals that for S_0 there is a local charge concentration in the non-bonded region of carbon, which does not appear in the S_1 state (fig. S10).

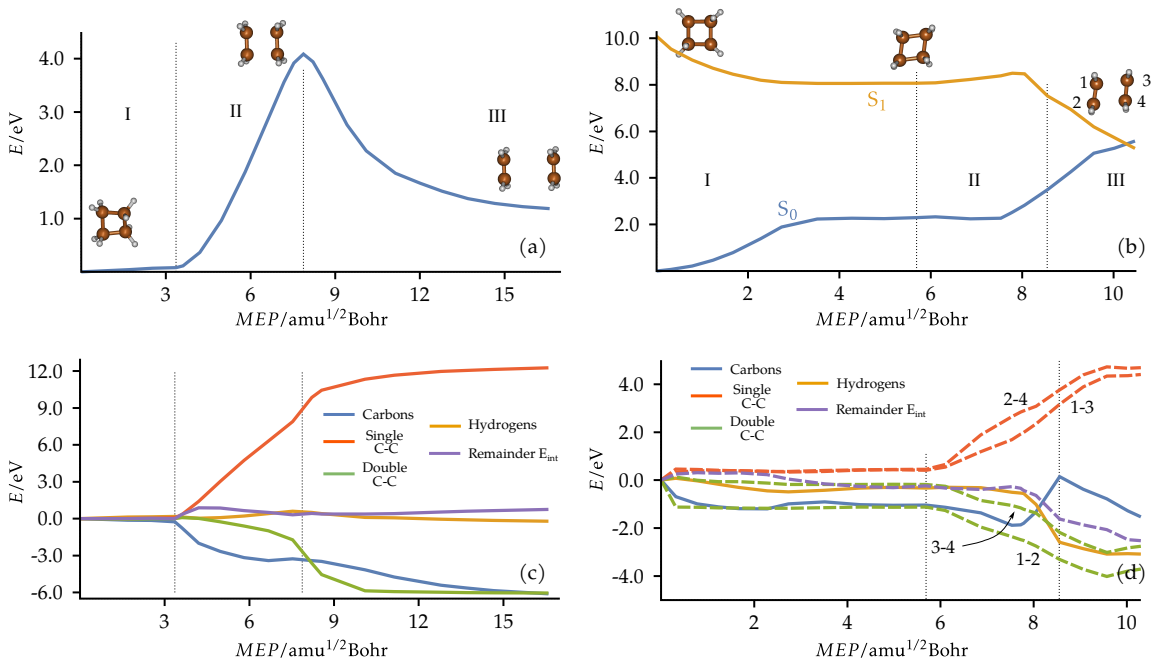

Figure 6: (a) Intrinsic reaction coordinate (IRC) for the ground state concerted dissociation of cyclobutane. (b) Energies of S_0 and S_1 along the minimum energy path of S_1. Changes on the self-energies and interaction energies (c) along the IRC for S_0 and (d) the MEP for S_1. The labels "Carbons" and "Hydrogens" comprise the sum of the deformation energies of the C or H atoms, respectively; "Remainder E_{int}" is the sum of the C-H and H-H interaction energies.

This information is congruent with a weakly bonded H$\cdots$CHO complex for S_1 and with HCO$\cdot$ + H$\cdot$ for S_0, and provides support for the roaming mechanism on S_1,[69,70] which arises as a dynamic effect connecting paths (15) and (16). Again, it should be noted that all of the above quantitative information is implicit in the description of the MEP, but cannot be trivially extracted from the analysis of the structures or the total energies in figure 5a. It is the use of the IQA/CASPT2 partition that facilitates the interpretation.

Regarding the reaction mechanism (16), previous studies suggest that the energy barriers involved are slightly lower on the triplet than on the singlet state.[64] The supporting information includes the analysis of the MEP for the $^3\pi\pi^\star$ state (figs. S11), which includes the change of surfaces from S_1 to T_1 through a minimum energy crossing point. The S_1/T_1 MECP was found at 1.13 eV from the minimum of $^1n\pi^\star$, whereas the subsequent T_1/S_0 MECP is at 0.95 eV from $^3\pi\pi^\star$, in agreement with previous reports for the molecule.[64] In

order to access to the S_1/T_1 MECP, it is necessary to pass from the pyramidalized structure of the $^1n\pi^\star$ energy minimum to a planar one, where the C-O distance goes from 1.35 Å to 1.70 Å. Therefore, in the region II shown in Fig. S7a the energetic changes associated with the elongation of the C-O contact are very similar to those of region I in Fig. 4a, i.e., more negative self-energies as well as a weakening of the C,O interaction. It is precisely the $E_{int}^{C,O}$ term which modulates the approach between the S_1 and T_1 surfaces and therefore, in mechanistic terms, favors the intersystem crossing.

Photodissociation of C_4H_8

Pericyclic photochemical reactions involving the cyclobutane moiety are relevant in materials science and biochemistry.[71–73] Unlike the cycloreversion for the Diels-Alder [4+2] reaction, the former is thermally forbidden but photochemically allowed and is thus complementary as a synthetic method in organic chemistry.[74] Following the transition of C_4H_8 to the first singlet excited state ($^1\sigma$R, Rydberg), the reaction path for the concerted dissociation proceeds favorably, involving a small energy barrier where the change of nature from $^1\sigma$R to $^1\sigma\sigma^\star$ takes place and ends at the crossing with the S_0 energy surface. Several theoretical methods have been applied in order to rationalize this process. For example, Geerlings has proposed an alternative interpretation of the Woodward-Hoffmann rules based on descriptors defined in conceptual density functional theory.[75] In this subsection, the IQA partition is used to approach the problem from a mechanistic viewpoint. The questions we seek to answer are: 1) Why is there a considerable energy barrier to the fragmentation of C_4H_8 if the rupture of two single bonds take place in a concerted step? and 2) Why the dissociation is more favorable in the excited state? For this purpose, the concerted photodissociation process is analyzed, instead of the birradical mechanism favored in the ground state.[76,77]

Figure 6a shows the intrinsic reaction coordinate (IRC) for the ground state concerted dissociation of cyclobutane, where a 4.08 eV energy barrier is observed. There are three well-defined regions on the IRC: the first one goes from 0 to 3.36 amu$^{1/2}$Bohr and involves

the passage from the puckered to a flat ring, where very small energy changes occur; in the second (3.36 to 7.87 amu$^{1/2}$Bohr), the distance between two C-C pairs begins to increase; and the third, where the dissociation into two C_2H_4 takes place. In terms of QTAIM molecular graphs, the structural catastrophe that marks the breaking of single bonds occurs between 12.01 and 12.79 amu$^{1/2}$Bohr. Because the carbon framework contributions are dominant and some components are related by symmetry, only the global contributions are presented in Fig. 6b. For example, the curve labeled "Carbons" involves the sum of the C self-energies. Proceeding from C_4H_8 to 2 C_2H_4 there is the breaking of two C-C single bonds, the formation of two double bonds as well as a formal change in hybridization from sp^3 to sp^2 in the four carbon atoms. Whereas the energy changes are positive for the former, they are negative for the latter. Briefly, the energy required for the concerted breaking of C-C single bonds exceeds the stabilization associated with the formation of two double bonds as well as the change in hybridization, thus explaining the appearance of the barrier. Near the TS structure, a change in the relevant electronic configuration describing the system takes place, going from $^1\sigma^2$ to $^1\sigma\sigma^\star$ from the C_4H_8 point of view ($^1\pi\pi^\star$ to $^1\pi^2$ for two C_2H_4), as reflected in the variation of the relevant molecular orbital occupation numbers (see fig. S12). Importantly, the change in electronic configuration describing the system at the TS coincides with the inflection point of the "Carbons", "Single C-C" and "Double C-C" curves (Fig. 6c).

The energy landscape changes considerably in the S_1 state. The $S_0 \rightarrow S_1$ electronic transition involves an excitation energy of 10.08 eV (0.05 oscillator strength). Subsequently, the MEP proceeds favorably until an energy minimum (0 to 5.69 amu$^{1/2}$Bohr), where the carbon framework changes from a puckered to a flat rhombus-shaped ring. In the second region of the MEP (5.69 to 8.55 amu$^{1/2}$Bohr) the change in nature (R $\rightarrow^1$ $\sigma\sigma^\star$) of the electronic state occurs, while the third ($>$ 8.55 amu$^{1/2}$Bohr) ends at the S_1/S_0 crossing. The energetic and structural changes in region I are driven by a decrease in the self-energies of the carbons and by the strengthening (more negative interaction energies) of one of the C,C bonded interactions which gains double bond character. Meanwhile, in II and III, the

cleavage of two single and the formation of two double bonds begins. Similar to the path at S_0, the stabilization gained by the formation of C=C contacts is smaller than the energy required to break two C-C bonds. However, note that near the transition state a considerable decrease in the hydrogen self-energies and from the C-H interactions occur, so that these contributions drive the MEP of S_1 towards the surface crossing, and therefore, promote the cycloreversion of the cyclobutane moiety. In other words, the IQA analysis reveals that the energy contributions "Hydrogens" and "Remaining E_{int}" are relevant to explain the deactivation of the excited state. This kind of information is not recovered from the analysis of the correlation diagram, which only focuses on the carbon-centered molecular orbitals and completely ignores the contributions of the hydrogens.

Conclusions

The implementation of the IQA energy partition using the one- and two-electron effective density matrices of the CASPT2 energy functional was carried out. The energy decomposition along a reaction path into IQA/CASPT2 contributions allows to describe in an orbital invariant language chemical transformations where strong correlation is important. This procedure provides a way of quantifying the main atomic and interaction contributions involved in electronic excitation and relaxation processes, possibly involving conical intersections or avoided crossings of states. The methodology was applied to several test systems. For example, the interaction contribution favors the formation of noble gas excimers and exciplexes, showing a predominant covalent character in the former and electrostatic in the latter. As another case, it was possible to establish that the C-O interaction in H_2CO dominates the S_1/S_0 and S_1/T_1 crossings. The study of the photodissociation of C_4H_8 shows that the contributions of the hydrogen atoms, usually not taken into account in the correlation diagram of the molecule, explains the small energy barrier in the lowest singlet electronic excited state. Finally, the comparison between the IQA/CASSCF and IQA/CASPT2 data

for H_2CO suggests the possibility of perform a qualitative description of a photophysical processes with the cheaper IQA/CASSCF approach, which would allow the study of large systems in the case where differential correlation effects are not important, i.e., CASSSCF and CASPT2 provide the same description of the PES. These examples show the usefulness of the IQA method in the mechanistic rationalization of photophysical and photochemical processes.

Author Contributions

J. J.-C.: Conceptualization, Project administration, Investigation, Writing - Original draft preparation. **E. L.-S.**: Investigation, Formal analysis, Writing - Original draft preparation. **J. P. P.**: Resources, Formal analysis, Visualization. **A. M. P.**: Resources, Formal analysis, Writing-Reviewing and Editing. **E. F.**: Investigation, Formal analysis, Software development. **J. H.-T.**: Conceptualization, Resources, Project administration, Writing - Original draft preparation.

Conflicts of interest

There are no conflicts to declare.

Acknowledgement

The authors thank DGTIC-UNAM for supercomputer resources (project LANCAD-UNAM-DGTIC-103) and financial support from UNAM-DGAPA (project PAPIIT IN112821). J. H.-T. thanks PAIP Facultad de Química UNAM (grant 5000-9004). J. P. P thanks "Laboratorio Nacional de Supercómputo del Sureste de México" (project 201903085N). J. J.-C. thanks CONACyT-México grant Ciencia de Frontera 2019-51496 and Patronato-UAN grant "Fortalecimiento a la Investigación". E. F. and A. M. P. thank the Spanish MICINN, grant

PGC2018-095953-B-I00, for funding.

Supporting Information Available

The following file is available free of charge.

- supplementary_information.pdf: Potential energy curves, complementary IQA energetic data and electronic descriptors (atomic charges) for all the studied systems.

References

(1) J. Andrés, P. W. Ayers, R. A. Boto, R. Carbó-Dorca, H. Chermette, J. Cioslowski, J. Contreras-García, D. L. Cooper, G. Frenking, C. Gatti, F. Heidar-Zadeh, L. Joubert, A. Martín Pendás, E. Matito, I. Mayer, A. J. Misquitta, Y. Mo, J. Pilmé, P. L. A. Popelier, M. Rahm, E. Ramos-Cordoba, P. Salvador, W. H. E. Schwarz, S. Shahbazian, B. Silvi, M. Sola, K. Szalewicz, V. Tognetti, F. Weinhold and E. L. Zins, *J. Comput. Chem.*, 2019, **40**, 2248–2283.

(2) M. A. Blanco, A. Martín Pendás and E. Francisco, *J. Chem. Theory Comput.*, 2005, **1**, 1096–1109.

(3) W. E. Vallejo Narváez, E. I. Jiménez, E. Romero-Montalvo, A. Sauza de la Vega, B. Quiroz-García, M. Hernández-Rodríguez and T. Rocha-Rinza, *Chem. Sci.*, 2018, **9**, 4402–4413.

(4) N. Orangi, K. Eskandari, J. C. R. Thacker and P. L. A. Popelier, *ChemPhysChem*, 2019, **20**, 1922–1930.

(5) V. M. Castor-Villegas, J. M. Guevara-Vela, W. E. Vallejo Narváez, A. Martín Pendás, T. Rocha-Rinza and A. Fernández-Alarcón, *J. Comput. Chem.*, 2020, **41**, 2266–2277.

(6) A. Silva, L. Duarte and P. L. A. Popelier, *Struct. Chem.*, 2020, **31**, 507–519.

(7) A. Fernández-Alarcón, J. L. Casals-Sainz, J. M. Guevara-Vela, A. Costales, E. Francisco, A. Martín Pendás and T. Rocha-Rinza, *Phys. Chem. Chem. Phys.*, 2019, **21**, 13428–13439.

(8) K. Szalewicz, *WIREs Comput. Mol. Sci.*, 2012, **2**, 254–272.

(9) M. J. S. Phipps, T. Fox, C. S. Tautermann and C.-K. Skylaris, *Chem. Soc. Rev.*, 2015, **44**, 3177–3211.

(10) A. Fernández-Alarcón, J. M. Guevara-Vela, J. L. Casals-Sainz, A. Costales, E. Francisco, A. Martín Pendás and T. Rocha-Rinza, *Chem. Eur. J.*, 2020, **26**, 17035–17045.

(11) J. Jara-Cortés, J. M. Guevara-Vela, A. Martín Pendás and J. Hernández-Trujillo, *J. Comput. Chem.*, 2017, **38**, 957–970.

(12) D. Ferro-Costas, A. Martín Pendás, L. González and R. A. Mosquera, *Phys. Chem. Chem. Phys.*, 2014, **16**, 9249–9258.

(13) R. Chávez-Calvillo, M. García-Revilla, E. Francisco, A. Martín Pendás and T. Rocha-Rinza, *Comput. Theo. Chem.*, 2015, **1053**, 90 – 95.

(14) J. L. McDonagh, M. A. Vincent and P. L. A. Popelier, *Chem. Phys. Lett.*, 2016, **662**, 228–234.

(15) F. J. Holguín-Gallego, R. Chávez-Calvillo, M. García-Revilla, E. Francisco, A. Martín Pendás and T. Rocha-Rinza, *J. Comput. Chem.*, 2016, **37**, 1753–1765.

(16) J. L. Casals-Sainz, J. M. Guevara-Vela, E. Francisco, T. Rocha-Rinza and A. Martín Pendás, *J. Comput. Chem.*, 2020, **41**, 1234–1241.

(17) P. Maxwell and P. L. A. Martín Pendás, A.and Popelier, *Phys. Chem. Chem. Phys.*, 2016, **18**, 20986–21000.

(18) E. Francisco, J. Casals-Sainz, T. Rocha-Rinza and A. Marín Pendás, *Theor. Chem. Acc.*, 2016, **135**, 170.

(19) B. Helmich-Paris, *J. Chem. Theory Comput.*, 2019, **15**, 4170–4179.

(20) K. Andersson, P. A. Malmqvist and B. O. Roos, *J. Chem. Phys.*, 1992, **96**, 1218–1226.

(21) L. Serrano-Andrés and M. Merchán, *J. Photochem. and Photobio. C*, 2009, **10**, 21–32.

(22) C. E. Crespo-Hernández, L. Martínez-Fernández, C. Rauer, C. Reichardt, S. Mai, M. Pollum, P. Marquetand, L. González and I. Corral, *J. Am. Chem. Soc.*, 2015, **137**, 4368–4381.

(23) M. K. MacLeod and T. Shiozaki, *J. Chem. Phys.*, 2015, **142**, 051103.

(24) N. Naoki and G. Sheng, *J. Chem. Phys.*, 2017, **146**, 094102.

(25) C. Song and T. J. Martínez, *J. Chem. Phys.*, 2018, **149**, 044108.

(26) R. F. W. Bader, *Atoms in Molecules: A Quantum Theory*, Clarendon Press, Oxford, 1990.

(27) J. M. Guevara-Vela, E. Francisco, T. Rocha-Rinza and A. Martín Pendás, *Molecules*, 2020, **25**, 4028.

(28) M. Gallegos, A. Costales and A. M. Pendás, *ChemPhysChem*, 2021, **22**, 775–787.

(29) A. M. Pendás and E. Francisco, *Phys. Chem. Chem. Phys.*, 2018, **20**, 16231–16237.

(30) T. Helgaker, P. Jorgensen and J. Olsen, *Molecular Electronic-Structure Theory*, Wiley, 2000.

(31) P. Pulay, *Int. J. Quantum Chem.*, 2011, **111**, 3273–3279.

(32) P. Celani and H.-J. Werner, *J. Chem. Phys.*, 2003, **119**, 5044–5057.

(33) B. O. Roos and K. Andersson, *Chem. Phys. Lett.*, 1995, **245**, 215–223.

(34) N. Forsberg and M. Per-Ake, *Chem. Phys. Lett.*, 1997, **274**, 196–204.

(35) J. Finley, P.-A. Malmqvist, B. O. Roos and L. Serrano-Andrés, *Chem. Phys. Lett.*, 1998, **288**, 299–306.

(36) S. Toru, G. Werner, P. Celani and W. Hans-Joachim, *J. Chem. Phys.*, 2011, **135**, 081106.

(37) W. Hans-Joachim, *Mol. Phys.*, 1996, **89**, 645–661.

(38) H. J. Werner, G. Knizia, F. R. Manby, M. Schütz, P. Celani, T. Korona, R. Lindh, A. Mitrushenkov, G. Rauhut, K. R. Shamasundar, T. B. Adler, R. D. Amos, A. Bernhardsson, A. Berning, D. L. Cooper, M. J. O. Deegan, A. J. Dobbyn, F. Eckert, E. Goll, C. Hampe and P. J. Knowles, *MOLPRO (versión 2010.26): a package of ab initio programs. www.molpro.net*, 2010.

(39) T. Shiozaki, *WIREs Comput. Mol. Sci.*, 2018, **8**, e1331.

(40) D. E. Woon and T. H. Dunning, *J. Chem. Phys.*, 1994, **100**, 2975–2988.

(41) F. Weigend and R. Ahlrichs, *Phys. Chem. Chem. Phys.*, 2005, **7**, 3297–3305.

(42) P. Oliveira, C. Barros, F. Jorge, A. Canal Neto and M. Campos, *J. Mol. Struc.*, 2010, **948**, 43–46.

(43) J. W. Raymonda, *J. Chem. Phys.*, 1972, **56**, 3912–3920.

(44) P. J. Knowles and N. C. Handy, *Comput. Phys. Commun.*, 1989, **54**, 75–83.

(45) A. Martín Pendás and E. Francisco, A QTAIM/IQA code (Available from the authors upon request).

(46) J. Vollbrecht, *New J. Chem.*, 2018, **42**, 11249–11254.

(47) I. Takashi and O. Shinji, *Nature*, 2000, **406**, 1027–1031.

(48) L. Forney, C. Moraru and T. Koutchma, *Ultraviolet Light in Food Technology: Principles and Applications*, CRC Press, 2009.

(49) M. Wolbarsht, *Laser Applications in Medicine and Biology*, Springer US, 2012.

(50) M. Diegelmann, W. G. Wrobel and K. Hohla, *Appl. Phys. Lett.*, 1978, **33**, 525–527.

(51) T. D. Bonifield, F. H. K. Rambow, G. K. Walters, M. V. McCusker, D. C. Lorents and R. A. Gutcheck, *J. Chem. Phys.*, 1980, **72**, 2914–2924.

(52) M. A. Slifkin, *Nature*, 1963, **200**, 766–767.

(53) J. B. Birks, *Rep. Prog. Phys.*, 1975, **38**, 903–974.

(54) W. C. Ermler, Y. S. Lee, K. S. Pitzer and N. W. Winter, *J. Chem. Phys.*, 1978, **69**, 976–983.

(55) P. Slavicek, R. Kalus, P. Paska, I. Odvárková, P. Hobza and A. Malijevský, *J. Chem. Phys.*, 2003, **119**, 2102–2119.

(56) A. M. Pendás, E. Francisco and M. A. Blanco, *J. Phys. Chem. A*, 2006, **110**, 12864–12869.

(57) R. A. Cox and G. D. Hayman, *Nature*, 1988, **332**, 796–800.

(58) M. J. Molina, *Angew. Chem. Int. Edit.*, 1996, **35**, 1778–1785.

(59) J. Kalinowski, M. Räsänen and R. Gerber, *Chem. Phys. Lett.*, 2012, **535**, 44–48.

(60) N. Turro, V. Ramamurthy and J. Scaiano, *Modern Molecular Photochemistry of Organic Molecules*, University Science Books, 2010.

(61) C. B. Moore and J. C. Weisshaar, *Annu. Rev. Phys. Chem.*, 1983, **34**, 525–555.

(62) Y. Haas, *Photochem. Photobiol. Sci.*, 2004, **3**, 6–16.

(63) M. Araujo, B. Lasorne, M. J. Bearpark and M. A. Robb, *J. Phys. Chem. A*, 2008, **112**, 7489–7491.

(64) S. Maeda, K. Ohno and K. Morokuma, *Adv. Phys. Chem.*, 2012, **2012**, 268124.

(65) K. Bastian C., S. Tim, W. Alec M. and P. G. Barratt, *J. Mol. Spectrosc.*, 2019, **362**, 61–68.

(66) C. M. Marian, *WIREs Comput. Mol. Sci.*, 2012, **2**, 187–203.

(67) M. B. Robin, *Higher Excited States of Polyatomic Molecules*, Academic Press, 1985, pp. 253–278.

(68) K. N. Walzl, C. F. Koerting and A. Kuppermann, *J. Chem. Phys.*, 1987, **87**, 3796–3803.

(69) B. C. Shepler, Y. Han and J. M. Bowman, *J. Phys. Chem. Lett.*, 2011, **2**, 834–838.

(70) M. Araújo, B. Lasorne, A. L. Magalhaes, M. J. Bearpark and M. A. Robb, *J. Phys. Chem. A*, 2010, **114**, 12016–12020.

(71) G. K. Kole, T. Kojima, M. Kawano and J. J. Vittal, *Angew. Chem. Int. Edit.*, 2014, **53**, 2143–2146.

(72) W. Fuss, *J. Photoch. Photobio. A*, 2015, **297**, 45–57.

(73) Y. Dou, S. Xiong, W. Wu, S. Yuan and H. Tang, *J. Photoch. Photobio. B*, 2010, **101**, 31–36.

(74) F. A. Carey and R. J. Sundberg, *Advanced Organic Chemistry: Part A: Structure and Mechanisms*, Springer US, 2010.

(75) P. Geerlings, P. W. Ayers, A. Toro-Labbé, P. K. Chattaraj and F. De Proft, *Acc. Chem. Res.*, 2012, **45**, 683–695.

(76) C. Doubleday, *J. Am. Chem. Soc.*, 1993, **115**, 11968–11983.

(77) W. M. Nigel, R. Lindh and G. Karlstrom, *Chem. Phys. Lett.*, 1998, **289**, 442–450.